Jonathan A. Malen[1]
Department of Mechanical Engineering,
UC Berkeley,
Berkeley, CA 94720
e-mail: jonmalen@andrew.cmu.edu

Kanhayalal Baheti
Department of Chemistry,
UC Berkeley,
Berkeley, CA 94720

Tao Tong

Yang Zhao

Department of Mechanical Engineering,
UC Berkeley,
Berkeley, CA 94720

Janice A. Hudgings
Department of Physics,
Mount Holyoke College,
South Hadley, MA 01075

Arun Majumdar[2]
Department of Mechanical Engineering,
UC Berkeley,
Berkeley, CA 94720

Optical Measurement of Thermal Conductivity Using Fiber Aligned Frequency Domain Thermoreflectance

Fiber aligned frequency domain thermoreflectance (FAFDTR) is a simple noncontact optical technique for accurately measuring the thermal conductivity of thin films and bulk samples for a wide range of materials, including electrically conducting samples. FAFDTR is a single-sided measurement that requires minimal sample preparation and no microfabrication. Like existing thermoreflectance techniques, a modulated pump laser heats the sample surface, and a probe laser monitors the resultant thermal wave via the temperature dependent reflectance of the surface. Via the use of inexpensive fiber coupled diode lasers and common mode rejection, FAFDTR addresses three challenges of existing optical methods: complexity in setup, uncertainty in pump-probe alignment, and noise in the probe laser. FAFDTR was validated for thermal conductivities spanning three orders of magnitude (0.1–100 W/m K), and thin film thermal conductances greater than 10 W/m^2 K. Uncertainties of 10–15% were typical, and were dominated by uncertainties in the laser spot size. A parametric study of sensitivity for thin film samples shows that high thermal conductivity contrast between film and substrate is essential for making accurate measurements. [DOI: 10.1115/1.4003545]

Keywords: thermal conductivity, thermal diffusivity, thermometry, photothermal, thermoreflectance, frequency domain

1 Introduction

Decades ago, thermal conductivity in solids was determined by measuring the temperature gradient produced by steady heat flux across a one-dimensional geometry. Thin films and high conductance samples are challenging for these techniques due to small absolute temperature differences. Transient methods with excitation time-scales similar to diffusion time-scales have been employed to generate sufficient thermal gradients [1,2]. This idea was extended to periodic excitation, so that lock-in amplifiers could be used to resolve smaller signal to noise ratios (SNRs) [3–7]. Of these techniques, the 3-omega method [6] is most common, but requires invasive and time consuming microfabrication of electrical heating/sensing elements on the sample surface, rendering scanning operations impossible and measurements of rough or electrically conductive samples challenging. Noncontact all-optical methods use an intensity modulated pump laser to heat the sample and a probe laser to measure the resultant thermal wave via the temperature dependant optical properties of the sample or surrounding medium. Although these optical techniques overcome 3-omega's shortcomings, they are typically exceedingly complex or are applicable to a limited range of materials. For example, time-domain thermoreflectance (TDTR) techniques [2,8–15] are highly accurate but require ultrafast laser pumping, sensitive pump-probe delay stages, and extensive postprocessing. Likewise, detection by the mirage effect [3,4] requires liquid helium environment for low temperature measurements, has reduced accuracy for samples with low thermal diffusivity [16], and is also sensitive to pump-probe alignment.

In this paper, we present the fiber aligned frequency domain thermoreflectance (FAFDTR), an alternative pump-probe optical technique that has enhanced simplicity without sacrificing predictive accuracy over a wide range of materials and films. We herein build on frequency domain thermoreflectance (FDTR) techniques that use carefully aligned, low-noise, free space cw [17–21] or pulsed [21] lasers and external modulation of the pump laser beam, usually with an acousto-optic modulator or an electro-optic modulator. FAFDTR utilizes instead inexpensive fiber coupled diode lasers. These lasers can be directly modulated via their drive current, eliminating the need for external modulators, and enabling perfect pump-probe alignment via a simple fiber coupler. A common mode rejection scheme is introduced to maintain accuracy in spite of the inherently high noise levels associated with diode lasers.

Fiber optics were earlier invoked to improve alignment in TDTR [22] and more recently with diode lasers to measure the thermal conductivity of an evaporated metal film coating the fiber tip [23]. FAFDTR uses two fiber coupled diode lasers that are merged into a single fiber and collimated into free space as perfectly aligned pump and probe beams. Absorption of the pump beam on the sample creates a temperature wave in the material that can be swept between 1D and 3D heating through varying the modulation frequency. Temperature oscillations at the surface cause its reflectance to change and therein periodically modulate the reflected probe beam. Both the amplitude of the thermal re-

[1]Corresponding author. Present address: Department of Mechanical Engineering, Carnegie Mellon, Department of Mechanical Engineering, Pittsburgh, PA 15213.
[2]Present address: U.S. Department of Energy, 1000 Independence Avenue SW, Washington, DC 20585.

Contributed by the Heat Transfer Division of ASME for publication in the JOURNAL OF HEAT TRANSFER. Manuscript received June 1, 2010; final manuscript received January 10, 2011; published online May 2, 2011. Assoc. Editor: Kenneth Goodson.

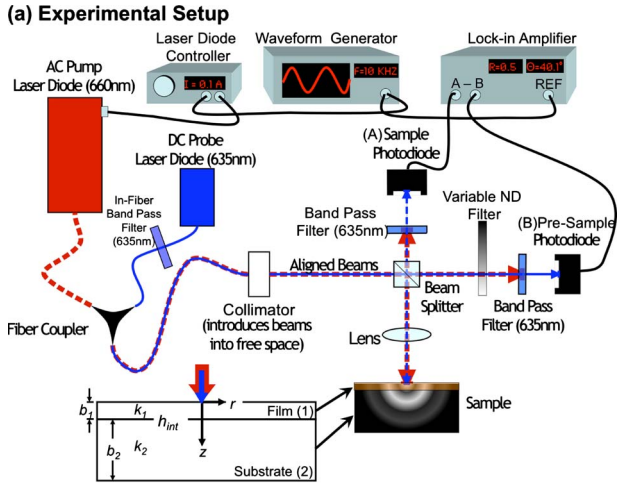

Fig. 1 Experimental setup and spot radius calibration. (*a*) FAFDTR uses fiber coupled diode lasers to produce pump (shown in red) and probe (shown in blue) beams of that are subsequently merged into a single fiber, leading to perfect pump-probe alignment at the sample surface. The pump power is periodically modulated (dashed line), resulting in a periodic temperature change of the sample surface. Due to the temperature dependant reflectivity of the sample, when the probe beam is reflected, it too becomes modulated. The phase lag between the periodic signals of the pump beam and reflected probe beam varies with modulation frequency and is used to evaluate the sample's thermal conductivity. Details of the setup are explained in the text. (*b*) CCD images of the pump beam reflected from patterned samples were used to determine the spot radius of our beam at the sample surface for 10×, 20×, and 50× lenses. Arrays of dots, with known dot-dot pitch (10 μm), were used for calibration. (Color online only.)

sponse and the phase lag between the pump and the temperature response depend on thermal conductivity, as previously demonstrated [17–20]. In this work, we monitor phase lag because it is less sensitive than amplitude to intensity instabilities that plague diode lasers.

Frequency dependent phase data from FAFDTR is fitted to a conduction model using the sample's thermal conductivity as the lone fitting parameter. The sample thermal conductivity is identified as the thermal conductivity providing the best match between model and experiment. Validation of FAFDTR is herein reported for both bulk and thin film samples with thermal conductivities spanning three orders of magnitude. A detailed error analysis is provided.

2 Experimental Setup

The experimental setup for FAFDTR is shown in Fig. 1(*a*). The pump is a high powered (~1 W max) 660 nm fiber coupled diode laser (Jenoptik). Its power is periodically modulated using an external laser diode controller (ILX Lightwave) driven by a waveform generator (National Instruments). The probe beam is a low powered (~5 mW max) 635 nm fiber coupled diode laser (Thorlabs), which emits a constant power beam. Both pump and probe beams are coupled into multimode fibers at the sources, and then merged into a single multimode fiber by a fused fiber coupler (OZ Optics). An in-line 635 nm bandpass filter is inserted between the probe laser and the fiber coupler to eliminate back reflection of the pump beam into the probe laser diode. The pump and probe beams exit into freespace through a collimator, as perfectly aligned parallel beams with Gaussian intensity profiles.

Once in free space, a beam-splitter samples 1% of the combined beams for presample noise measurement by photodiode (PD) B (Thorlabs PDA36A). The remaining 99% is directed through a microscope objective lens to the sample surface. Objectives of 10×, 20×, and 50× magnifications were used in the current study. In order to identify the spot size, reference samples patterned with regularly spaced grids were fabricated. The reflected image of the focused spot on the patterned surface is shown in Fig. 1(*b*).These images, taken by a CCD camera, were fitted using the Gaussian intensity distributions $\Gamma(r) \propto e^{-(r^2/r_{\text{spot}}^2)}$. Our fits indicate that the spot radii are 56 ± 3 μm, 26 ± 1.3 μm, and 9.6 ± 0.5 μm for 10×, 20×, and 50× objectives, respectively. The error represents the 95% confidence interval of the spot radius, accounting for deviations that may result when focusing onto unpatterned samples.

The focused pump beam imparts a periodic heat flux on the sample surface that results in a periodic temperature change within the sample. The phase and amplitude of temperature, relative to the heat flux, at the sample surface are related to the sample's thermal properties (thermal conductivity k, heat capacity c_p, and density ρ). The periodic temperature variation in the top layer $T_{1,\omega}$ results in a periodic change in the reflectivity of the surface R_ω due to the temperature dependence of reflectivity. The coefficient of thermoreflectance, $\beta(\lambda_{\text{probe}})$, defined as $\beta(\lambda_{\text{probe}}) = [1/R_0(\lambda_{\text{probe}})][dR(\lambda_{\text{probe}})/dT]$, quantifies the change in reflectivity as a function of temperature, where $R_0(\lambda_{\text{probe}})$ is the nominal reflectivity of the surface at the probe wavelength. Note that $\beta(\lambda_{\text{probe}})$ depends strongly on both the choice of sample material and the probe wavelength.

Hence, the periodic reflectivity variation is written in terms of the periodic temperature variation $T_{1,\omega}$ as

$$R_\omega = \beta(\lambda_{\text{probe}}) R_0(\lambda_{\text{probe}}) T_{1,\omega} \tag{1}$$

When the probe beam is reflected from the surface, it will pick up a small periodic signal due to R_ω.

$$I_{\text{signal},\omega} = I_{\text{probe}} R_\omega \tag{2}$$

The amplitude of $I_{\text{signal},\omega}$ is sensitive to instabilities in the probe laser power so we instead monitor the phase of $I_{\text{signal},\omega}$ relative to the pump $I_{\text{pump},\omega}$; this phase difference is directly related to the thermal conductivity of the sample. The postsample beams are reflected back through the beam-splitter and then through a 635 nm bandpass filter so that only the probe beam reaches photodiode A. The phase of the voltage signal from photodiode A is measured using a lock-in amplifier (SR830 Stanford Research Systems) and is mathematically defined as $\phi_{\text{signal}} = \tan^{-1}[\text{Im}(I_{\text{signal},\omega})/\text{Re}(I_{\text{signal},\omega})]$.

The local steady state temperature rise of the sample can be estimated as $\Delta T_{\text{avg}} = Q_{\text{avg}}/(2\sqrt{2}\pi r_{\text{spot}} k)$, where Q_{avg} is the time-averaged laser power absorbed by the sample [10], for example, for a typical Si sample with $k = 137$ W/m K, $r_{\text{spot}} = 9.6$ μm, and $Q_{\text{avg}} = 50$ mW, and has $\Delta T_{\text{avg}} = 7.6$ K. Caution should be taken to minimize ΔT_{avg} for low thermal conductivity samples by using low pump laser power or low duty-cycle periodic modulation that result in low Q_{avg}. For the room temperature validation results presented here, ΔT_{avg} was maintained below 10 K.

3 Signal to Noise Ratio Considerations

Although the exact amplitude of $I_{\text{signal},\omega}$ is not used by FAFDTR, its order of magnitude is important for achieving adequate SNRs. Favorable SNRs result from optimizing FAFDTR's signal strength and rejecting noise. Higher magnification lenses give FAFDTR higher SNRs because the same power focused into a smaller spot that generates higher heat flux and increased am-

plitudes of $T_{1,\omega}$ and $I_{\text{signal},\omega}$. In particular, higher magnification can be used to improve the SNR of high conductivity samples, where the amplitude of $T_{1,\omega}$ is small because it is inversely proportional to k (as later demonstrated mathematically by Eqs. (6) and (7)).

FAFDTR's signal amplitude can be further optimized by proper selection of the pump wavelength λ_{pump}, probe wavelength λ_{probe}, and surface coating. The observed periodic signal intensity $I_{\text{signal},\omega}$ is related to $T_{1,\omega}$ by combining Eqs. (1) and (2),

$$I_{\text{signal},\omega} = I_{\text{probe}} R_0(\lambda_{\text{probe}}) \beta(\lambda_{\text{probe}}) T_{1,\omega} \tag{3}$$

where the expression for R_ω was substituted from Eq. (1). The amplitude of $T_{1,\omega}$ is proportional to the periodic heat flux absorbed by the sample $I_{\text{pump},\omega} A_0(\lambda_{\text{pump}})$, where A_0 is the nominal absorptivity of the sample. The complete expression describing the signal strength in terms of wavelength dependant optical properties is

$$I_{\text{signal},\omega} \propto I_{\text{probe}} R_0(\lambda_{\text{probe}}) \beta(\lambda_{\text{probe}}) I_{\text{pump},\omega} A_0(\lambda_{\text{pump}}) \tag{4}$$

High β is sought by optimizing the choice of λ_{probe} for a given test material, but for similar pump and probe wavelengths, absorptivity and reflectivity are related by $A_0(\lambda_{\text{pump}}) \approx 1 - R_0(\lambda_{\text{probe}})$; their product is maximized when both equal 0.5. If the wavelengths of the pump and probe beams differ significantly, then R_0 and A can be independently maximized. Niobium adheres well to most sample surfaces and has optimal characteristics for our wavelengths: β peaked near the probe wavelength of 635 nm ($\beta \sim 1 \times 10^{-3}$ K^{-1} [24]), and the product of $R_0(\lambda_{\text{probe}}) A_0(\lambda_{\text{pump}})$ nearly maximized. For our samples, an optically thick 100 nm niobium film was deposited from a 99.99% niobium wire at a pressure of $\sim 2 \times 10^{-6}$ torr, with argon flow, sample chilled to 288 K, and a deposition rate of ~ 1 Å/s using an Edwards Auto dc Sputter Coater. The niobium thickness was measured directly using a contact profilometer with an experimental error of ~ 1 nm. This film has little effect on thermal response over our frequency range, but maximizes $I_{\text{signal},\omega}$ based on Eq. (4).

A common mode rejection scheme was employed to reject noise inherent to the probe laser by subtracting the presample probe beam from the postsample probe beam. When measured by a lock-in amplifier, the presample probe beam (photodiode B) contains substantial noise at the pump's modulation frequency. Since this noise originates in the probe laser diode, it is present in both pre and postsample beams. It is rejected by subtracting the presample signal (photodiode B) from the postsample signal (photodiode A). The periodic voltage signals from photodiodes A and B,

$$\begin{aligned} V_{A,\omega} &= V_{\text{signal}} \sin(\omega t + \phi_{\text{thermal signal}} + \phi_{\text{pump laser}} + \phi_{\text{PD-A}}) \\ &\quad + V_{\text{probe noise-A}} \sin(\omega t + \phi_{\text{probe noise}} + \phi_{\text{PD-A}}) V_{B,\omega} \\ &= V_{\text{probe noise-B}} \sin(\omega t + \phi_{\text{probe noise}} + \phi_{\text{PD-B}}) \end{aligned} \tag{5}$$

include phase lag from the following sources: (i) the thermal signal itself, (ii) pump laser response, (iii) PD response, and (iv) probe laser noise. Subtraction of the signals is performed using the SR830 lock-in amplifier's A-B setting ($V_{A,\omega} - V_{B,\omega}$). The A-B setting uses a low-noise differential amplifier to subtract input B from input A before passing the signal to the phase sensitive detector. Complete rejection requires that the observed noise intensity is equal at both photodiodes, and that both photodiodes have well matched responsivity ($V_{\text{noise-A}} = V_{\text{noise-B}}$) and response times ($\phi_{\text{PD-A}} = \phi_{\text{PD-B}}$) in the frequency range of interest. A variable neutral density filter, placed in front of photodiode B, was adjusted until $V_{\text{noise-A}} = V_{\text{noise-B}}$. Response times of our photodiodes (Thorlabs PDA36A), which have a bandwidth of 17 MHz, maintain $\phi_{\text{PD-A}} - \phi_{\text{PD-B}} < 1$ deg for the applicable frequency range (10 Hz–100 kHz). To isolate ϕ_{signal}, we made separate measurements of the pump beam to identify $\phi_{\text{PD-A}} + \phi_{\text{laser}}$, and subtracted it from the total phase observed by A-B. Our signal to noise ratio improved by an order of magnitude due to this rejection.

4 Frequency Domain Thermal Response of the Sample

An analytical expression for the frequency domain temperature response of a multilayered structure, subjected to periodic surface heating by Gaussian laser spot, was determined by Cahill [10] using the iterative algorithm of Feldman [25]. When probed by Gaussian laser spot of equal radius, the weighted average periodic temperature change is

$$\bar{T}_{1,\omega} = 2\pi Q_{\text{Per}} \int_0^\infty G(s) \exp(-\pi^2 s^2 2 r_{\text{spot}}^2) s ds \tag{6}$$

where $G(s)$ for a single layered sample is defined as

$$G(s)_{\text{1-layer}} = \frac{1}{k(4\pi^2 s^2 + i\omega/\alpha)^{1/2}} \tag{7}$$

Expressions for a multilayered sample are given by Eqs. (14)–(18) in Ref. [10]. FAFTDR phase data spanning a wide range of frequencies were fitted using Eq. (6) by varying the thermal conductivity of the unknown layer until the least-squares regression was minimized. Note that Cahill's definition of spot size is based on the $1/e^2$ radius and is related to our spot size as $r_{\text{Cahill}} = \sqrt{2} r_{\text{spot}}$, resulting in a factor of 2 in the exponent of Eq. (6) and a factor of $\sqrt{2}$ in the expression for ΔT_{avg}.

The frequency domain response can be qualitatively understood using simple analytical expressions for planar heating with 1D heat flow, and point heating with 3D heat flow in a single layer semi-infinite solid. For planar heating with incident heat flux $q_\omega(z=0) = q_{\text{Per}} \exp(i\omega t)$, the one-dimensional heat conduction equation in Cartesian coordinates can be analytically solved to yield the temperature at the surface,

$$T_{\text{planar},\omega}(z=0) = \frac{q_{\text{Per}}}{\sqrt{k\rho c_p \omega}} \exp[i(\omega t - \pi/4)] \tag{8}$$

where the amplitude of the surface temperature is inversely proportional to $\sqrt{\omega}$, and its phase lags the incident heat flux by $\pi/4$ (45 deg). In contrast, for point heating with incident power $Q_\omega(r=0) = Q_{\text{Per}} \exp(i\omega t)$, the heat conduction equation in spherical coordinates can be analytically solved to yield the 3D temperature distribution near to the heating point,

$$T_{\text{point},\omega}(r \to 0) = \frac{Q_{\text{Per}}}{2\pi k r} \exp(i\omega t) \tag{9}$$

where the amplitude is independent of ω and the phase is synchronous with the incident heat flux.

For our finite spot size, the phase lag of the temperature relative to the heat flux is between 0 deg and 45 deg. The precise value of the phase lag depends on the characteristic length scale of the thermal wave, which decays exponentially into the solid. This length scale, known as the thermal penetration depth, is defined as

$$L_p = \sqrt{2\alpha/\omega} \tag{10}$$

and is inversely proportional to ω. The ratio of L_p and r_{spot} determines whether the isotherms are relatively planar or are more spherical. If $r_{\text{spot}} \ll L_p$, the isotherms within the substrate are more spherical, the surface phase lag is ~ 0 deg, and Eq. (6) simplifies to Eq. (9) for point heating. Alternatively, if $r_{\text{spot}} \gg L_p$, the isotherms within the substrate are relatively planar, the surface phase lag is ~ 45 deg, and Eq. (6) simplifies to Eq. (8) for planar heating. As the heating frequency is increased, L_p decreases while r_{spot} remains constant, resulting in increasing phase lag. Materials with high k will have larger L_p and therefore smaller phase lags over a given frequency range than materials with low k. Experimentally, it is important to choose the frequency range, based on a comparison of L_p and r_{spot}, so that the phase will transition between 0 deg and 45 deg (in some cases (e.g., Si), the 100 kHz frequency limit of our lock-in amplifier made it experimentally impossible to sample the upper phase range).

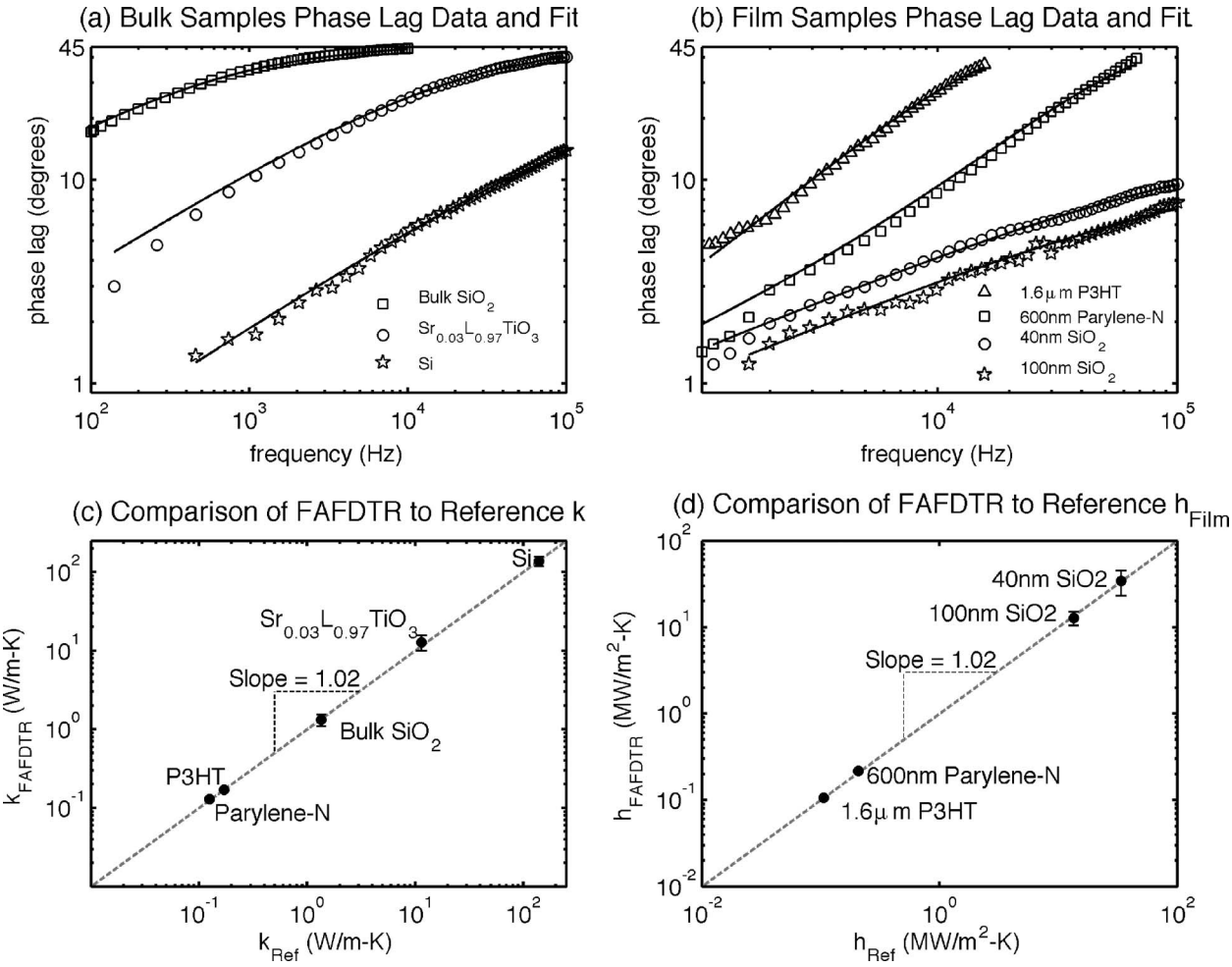

Fig. 2 FAFDTR data, fits, and comparison to reference samples. (*a*) Measured phase lag between the surface temperature and the applied heat flux for bulk samples; solid lines show the best fit of the model to the experimental data. (*b*) Phase lag data and best fit for thin film samples. (*c*) Comparison between thermal conductivity measured by FAFDTR (k_{FAFDTR}) and the reference thermal conductivity of our samples (k_{ref}). A linear fit to these points has a slope of 1.02, indicating that FAFDTR is accurate for measurement of $k \sim 0.1-100$ W/m K. (*d*) FAFDTR's ability to measure high thermal conductance thin film samples is demonstrated by comparing the reference thermal conductance ($h_{ref}=k_{ref}/L_{film}$) to the FAFDTR prediction of thermal conductance ($h_{FAFDTR}=k_{FAFDTR}/L_{film}$). A linear fit to these points has a slope of 1.02, indicating that FAFDTR is accurate for measurement of $h_{film} \sim 0.1-35$ W/m K.

5 Validation of FAFDTR with Bulk and Thin Film Reference Samples

Bulk samples (i.e., having thicknesses much greater than L_p) of amorphous silicon dioxide SiO_2, $Sr_{0.03}La_{0.97}TiO_3$ (SLTO), and single-crystal silicon (Si) coated with 100 nm thick Nb films were measured. Data and fits of phase lag, based on Eq. (6) with best matched k_{sub}, are shown in Fig. 2(*a*). As anticipated, the phase lag increases asymptotically to 45 deg as frequency is increased. The extracted values of k_{sub} are compared with reference values in Table 1; the reported uncertainties are discussed in the uncertainty analysis section. Measured values of r_{spot} and literature values of the specific heat and density of our samples [26] were assumed as fixed inputs to the model, and are listed in Table 1. In most cases, the interface resistance between the Nb film and the bulk sample is expected to be negligibly small. One exception is the Si substrate; the thin native SiO_2 layer ($\sim$1 nm) between the Nb film and our Si reference samples resulted in a well studied thermal resistance at the interface between Si and SiO_2 [27–29]. For thermally grown SiO_2, an interface conductance of $h_{int} \sim 30$ MW/m^2 K has been recently reported [28,29] and was assumed here.

FAFDTR was also validated against four thin films on Si substrates. Samples included thermally grown SiO_2 films of 40n m and 100 nm, a 600 nm parylene film, and a 1.6 μm poly-3-hexylthiophene (P3HT) film. The SiO_2 films were measured using a NanoSpec film thickness measurement system. The parylene was deposited using a PDS 2010 Labcoter 2 made by Specialty Coating Systems. The deposition process evaporates a precursor that is pyrolized leaving parylene-n deposited on the surface. The P3HT was purchased from Sigma Aldrich, dissolved in chloroform, and dropcast onto the sample surface following the preparation from [30]. The thicknesses of parylene and P3HT films were measured directly using a contact profilometer with experimental error of $\sim$1 nm.

FAFDTR data and fits of phase lag, based on Eq. (6) with best matched k_{film}, are shown in Fig. 2(*b*) for all films. The extracted values of k_{film} are compared with reference values in Table 1. For the SiO_2 films, an interface conductance of $h_{int} \sim 30$ MW/m^2 K was again used. For the polymer films, the interface conductance is much higher than the film conductance and hence did not sensitively influence evaluation of the film properties.

For k spanning three orders of magnitude, FAFDTR's estimate

Table 1 Comparison of FAFDTR with reference samples. Thermal conductivities measured by FAFDTR are compared with reference thermal conductivities. The reported uncertainty in k_{FAFDTR}, derived in the uncertainty analysis, results from the reported uncertainties in the modeling parameters.

		Thermal conductivity		Modeling parameters			
Sample		k_{FAFDTR} (W/m K)	$k_{reference}$ (W/m K)	r_{spot} (μm)	ρ (kg/m^3)	c_p (J/kg K)	h_{int} (MW/m^2 K)
Bulk	Bulk SiO_2	1.32 ± 0.18	1.3 [32]	26.0 ± 1.3 (20×)	2220 ± 22	745 ± 7	100 ± 30 [a]
	$Sr_{0.03}La_{0.97}TiO_3$	11.6 ± 1.3	11.5 [33]	9.6 ± 0.5 (50×)	5130 ± 51	546 ± 5	100 ± 30 [a]
	Si	137 ± 18	142 [34]	9.6 ± 0.5 (50×)	2330 ± 23	712 ± 7	30 ± 10 [b]
Thin film (Si substrate)	600 ± 6 nm parylene	0.13 ± 0.003	0.13 [35]	56.0 ± 3 (10×)	1300 ± 13	1700 ± 17	100 ± 30 [a]
	1600 ± 12 nm P3HT	0.17 ± 0.004	0.17	56.0 ± 3 (10×)	1330 ± 13	1200 ± 12	100 ± 30 [a]
	40 ± 1 nm thermal SiO_2	1.37 ± 0.42	1.3 [32]	9.6 ± 0.5 (50×)	2220 ± 22	745 ± 7	30 ± 10 [b]
	100 ± 1 nm thermal SiO_2	1.29 ± 0.21	1.3 [32]	9.6 ± 0.5 (50×)	2220 ± 22	745 ± 7	30 ± 10 [b]

[a]Interface thermal conductance of 100 ± 30 MW/m^2 K was assumed between Nb coating or thin film and substrate. This value is typical of metal-insulator interfaces [36] but plays a limited roll as k_{FAFDTR} was insensitive to its value, as shown in Table 2.
[b]Interface thermal conductance of 30 ± 10 MW/m^2 K was assumed between Si and native or thermally grown SiO_2 layer [28,29].

(k_{FAFDTR}) is in agreement with the reference (k_{ref}). These results are summarized in Fig. 2(*c*); k_{FAFDTR} is plotted against k_{ref}, and the data fall on the line with slope equals unity. Figure 2(*d*) compares $h_{FAFDTR}=k_{FAFDTR}/L_{film}$ to $h_{ref}=k_{ref}/L_{film}$ to demonstrate FAFDTR's utility in evaluating thin film or interface conductances in excess of 30 MW/m^2 K.

6 Uncertainty Analysis

An uncertainty analysis was performed to evaluate the uncertainty in FAFDTR's prediction of thermal conductivity and as guidance to further applications of FAFDTR. Uncertainties of 10–15% were typical for our samples. Comparable uncertainties are typical of 3-omega and TDTR [31], making FAFDTR an attractive alternative given its simplicity and range. The dominant source of uncertainty was the size of the applied hot spot r_{spot}, as we explain next.

The uncertainty Δk_i in FAFDTR's evaluation of thermal conductivity k_i of layer i was estimated from the uncertainties in the modeling parameters j:

$$\Delta k_i = \sqrt{\sum_j (\Delta k_i^j)^2} \quad \Delta k_i^j = \frac{\partial k_i}{\partial j}\Delta j$$

$$j = r_{spot}, L_{film}, c_{p,film}, \rho_{film}, c_{p,sub}, \rho_{sub}, h_{int}, k_{j\neq i} \tag{11}$$

where $k_{j\neq i}$ implies that we consider uncertainty in the thermal conductivity of the substrate when determining the thermal conductivity of the film and vice versa. Since the pump and probe beams are concentric, the uncertainty due to misalignment of the spots is considered negligible. The uncertainty in k_i due to a single input parameter is Δk_i^j and depends on the sensitivity of k_i to that parameter $\partial k_i/\partial j$, as well as the uncertainty in that parameter Δj. Numerically, we evaluate Δk_i using the following three step procedure: (1) use least-squares regression to determine k_i providing the best match between the phase angle of $T_{1,\omega}$ and ϕ_{signal} data, given nominal values of the modeling parameters; (2) perturb one modeling parameter j by a quantity Δj (its uncertainty) and repeat step 1 to determine the difference in k_i that results from a known change to j, i.e., Δk_i^j; (3) repeat steps 1 and 2 to determine all Δk_i^j and take the square root of the sum of squares to evaluate the total uncertainty in Δk_i. This procedure automatically incorporates uncertainty due to random noise in the phase data or inaccuracy of fit. For the validation samples, our reported uncertainty in k is based on estimated uncertainties in r_{spot} and h_{int} from Table 1, as well as 1% uncertainties in the values of L_{film}, $c_{p,film}$, ρ_{film}, $c_{p,sub}$, ρ_{sub}, and $k_{j\neq i}$. For bulk samples, our uncertainty is less than 14%, which is comparable to the uncertainty of TDTR and 3ω.

A sensitivity analysis clarifies the sources of uncertainty in FAFDTR's predictions of thermal conductivity. The sensitivity is quantified as the percent change in k_i due to 1% change in the parameter j, and was calculated using steps 1 and 2 of the procedure listed above (with $\Delta j/j=0.01$). Table 2 lists the sensitivities and shows that in general k_i is most sensitive to r_{spot}, which is itself a relatively difficult parameter to measure precisely. Although r_{spot} is the dominant source of uncertainty in k_i, caution must be taken to identify other sensitive parameters subject to the specifics of the measurement setup and unknown sample. For example, Table 2 also shows that very thin films are highly sensitive to the substrate thermal conductivity.

Table 2 Sensitivity analysis. The percent change in k_{FAFDTR} due to a 1% change in the specified modeling parameters. For example, for bulk SiO_2, a 1% change in the value of $k_{Nb\ film}$ results in a 0.28% change in k_{FAFDTR}, the extracted thermal conductivity of the bulk SiO_2. In general, k_{FAFDTR} is most sensitive to uncertainty in r_{spot}, but caution must be taken to identify other sensitive parameters subject to the specifics of the measurement setup and the unknown sample.

Sample		$k_{Nb\ film}$	$k_{Si\ sub}$	b_{film}	r_{spot}	ρ	c_p	h_{int}
Bulk	Bulk SiO_2	0.28	—	0.18	2.75	0.88	0.88	0.27
	$Sr_{0.03}La_{0.97}TiO_3$	0.1	—	0.01	2.09	0.69	0.69	0.01
	Si	0.05	—	0.06	1.44	0.49	0.49	0.46
Thin film (Si substrate)	600 ± 6 nm parylene	—	0.05	2.1	0.02	1.09	1.09	0.01
	1600 ± 12 nm P3HT	—	0.05	2.09	0.04	1.08	1.08	0.01
	40 ± 1 nm thermal SiO_2	—	3.8	0.93	4.86	0.07	0.07	1.22
	100 ± 1 nm thermal SiO_2	—	2.29	0.85	2.87	0.14	0.14	0.44

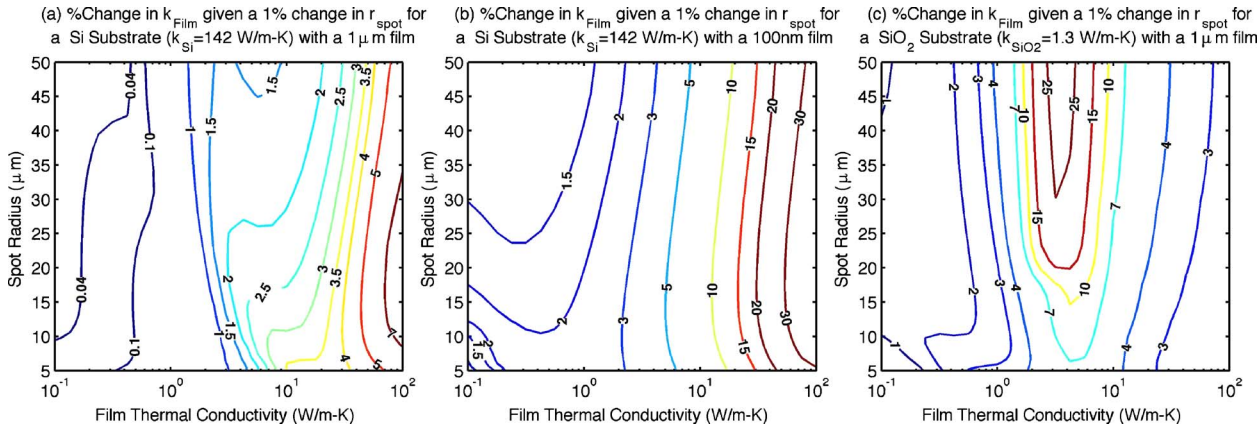

Fig. 3 Sensitivity of FAFDTR to uncertainty in heating spot radius for thin film samples. Subplots (*a*)–(*c*) correspond to the percent uncertainty in k_{film} due to a 1% uncertainty in r_{spot} for cases (*a*)–(*c*) discussed in the text. Contours of percent uncertainty are labeled. Using case (*a*) as an example, the contours can be interpreted as follows: For r_{spot} of 10 μm and k_{film} of 10 W/m²-K, there will be an ~3% uncertainty in k_{film}, given a 1% uncertainty in r_{spot}. High uncertainty results when the thermal conductivities of the film and substrate are similar.

As a guidance to minimize uncertainty for future applications of FAFDTR to thin film measurements, we have performed a parametric study to quantify the sensitivity of k_{film} to r_{spot}, for a range of k_{film} and r_{spot}. The following three cases were considered: (a) a silicon substrate with a 1 μm film, (b) a silicon substrate with 100 nm film, and (c) a SiO_2 substrate with a 1 μm film. The uncertainty in k_{film} was determined by (1) calculating ϕ_{signal} over a range of frequencies for a nominal combination of r_{spot} and k_{film}; (2) perturbing r_{spot} by 1% and then calculating the compensating change in k_{film} required to fit ϕ_{signal} from step 1, and (3) repeating for each combination of r_{spot} and k_{film}. The results are summarized as contour plots as a function of r_{spot} and k_{film} in Fig. 3, where subplots a–c correspond to cases a–c. Using case (a) as an example, the contours can be interpreted as follows: for r_{spot} of 10 μm and k_{film} of 10 W/m K, there will be a ~3% uncertainty in k_{film}, given a 1% uncertainty in r_{spot}. The primary trend, shown by the contour plots, is that the sensitivity of k_{film} to uncertainty in r_{spot} increases dramatically when k_{film} and k_{sub} are similar. A secondary trend is that increased film thickness reduces the sensitivity of k_{film} to uncertainty in r_{spot}. The contours are roughly independent of the nominal value of r_{spot}. Hence, for accurate characterization of k_{film}, thick films and substrates with high thermal conductivity contrast between film and substrate are recommended.

7 Conclusions

We have developed a noncontact optical technique for measurement of thermal conductivity in thin films and bulk samples. The technique uses fiber aligned diode lasers to pump and probe temperature changes at the sample surface. Fiber alignment eliminates uncertainty due to pump-probe misalignment, and the complexity needed to otherwise overcome it. Phase lag of temperature (relative to heat flux), instead of amplitude, is monitored for thermal conductivity prediction because it is insensitive to the sample's optical properties or variations in laser intensity that otherwise add uncertainty. We have validated FAFDTR for thermal conductivities spanning three orders of magnitude (0.1–100 W/m K), and thin film thermal conductances greater than 30 MW/m² K. Uncertainties of 10–15% were typical and are dominated by uncertainties in determining the laser heating spot size. A parametric study of sensitivity for thin film samples shows that high thermal conductivity contrast between film and substrate is essential for making accurate measurements.

Acknowledgment

We thank Rajeev Ram and Jason Orcutt from MIT for insightful conversations and advice that benefited this work.

Nomenclature

A_0 = nominal absorptivity
b = thickness (m)
c_p = specific heat (J/kg K)
h = thermal conductance (W/m² K)
I = optical signal (W)
k = thermal conductivity (W/m K)
L_p = thermal penetration depth (m)
Q = absorbed laser power (W)
q = heat flux (W/m²)
r = radial position from center of spot (m)
r_{spot} = laser spot radius (m)
R_0 = nominal reflectivity
s = Integration variable for Eq. (6)
t = time (s)
T = temperature (K)
V = voltage signal (V)
z = axial position from sample surface (m)
α = thermal diffusivity (m²/s)
β = coefficient of thermoreflectance (K^{-1})
ϕ = phase lag (deg)
λ = wavelength (m)
ρ = density (kg/m³)
ω = frequency (rads/s)
Γ = normalized radial distribution (m^{-2})

Subscripts

avg = amplitude of a constant signal
FAFDTR = FAFDTR prediction
film = thin film
i = layer index (i=1,2,3), where layer 1 is the Nb film
int = interface
j = modeling parameter index for uncertainty analysis
Nb = niobium
per = amplitude of a periodic signal
ref = reference value
sub = substrate

ω = variable is periodic in time

References

[1] Parker, W. J., Jenkins, R. J., Abbott, G. L., and Butler, C. P., 1961, "Flash Method of Determining Thermal Diffusivity, Heat Capacity, and Thermal Conductivity," J. Appl. Phys., **32**(9), pp. 1679–1684.

[2] Paddock, C. A., and Eesley, G. L., 1986, "Transient Thermoreflectance From Thin Metal-Films," J. Appl. Phys., **60**(1), pp. 285–290.

[3] Boccara, A. C., Fournier, D., and Badoz, J., 1980, "Thermooptical Spectroscopy—Detection by the Mirage Effect," Appl. Phys. Lett., **36**(2), pp. 130–132.

[4] Murphy, J. C., and Aamodt, L. C., 1980, "Photothermal Spectroscopy Using Optical Beam Probing—Mirage Effect," J. Appl. Phys., **51**(9), pp. 4580–4588.

[5] Rosencwaig, A., Opsal, J., Smith, W. L., and Willenborg, D. L., 1985, "Detection of Thermal Waves Through Optical Reflectance," Appl. Phys. Lett., **46**(11), pp. 1013–1015.

[6] Cahill, D. G., 1990, "Thermal-Conductivity Measurement From 30-K to 750-K—The 3-Omega Method," Rev. Sci. Instrum., **61**(2), pp. 802–808.

[7] Ohsone, Y., Wu, G., Dryden, J., Zok, F., and Majumdar, A., 1999, "Optical Measurement of Thermal Contact Conductance Between Wafer-Like Thin Solid Samples," ASME J. Heat Transfer, **121**(4), pp. 954–963.

[8] Cahill, D. G., Ford, W. K., Goodson, K. E., Mahan, G. D., Majumdar, A., Maris, H. J., Merlin, R., and Phillpot, S. R., 2003, "Nanoscale Thermal Transport," J. Appl. Phys., **93**(2), pp. 793–818.

[9] Anderson, A. C., and Wolfe, J. P., 1986, *Phonon Scattering in Condensed Matter V: Proceedings of the Fifth International Conference*, Urbana, IL, Jun. 2–6, Springer-Verlag, Berlin.

[10] Cahill, D. G., 2004, "Analysis of Heat Flow in Layered Structures for Time-Domain Thermoreflectance," Rev. Sci. Instrum., **75**(12), pp. 5119–5122.

[11] Cahill, D. G., Goodson, K., and Majumdar, A., 2002, "Thermometry and Thermal Transport in Micro/Nanoscale Solid-State Devices and Structures," ASME J. Heat Transfer, **124**(2), pp. 223–241.

[12] Käding, O. W., Skurk, H., and Goodson, K. E., 1994, "Thermal Conduction in Metallized Silicon-Dioxide Layers on Silicon," Appl. Phys. Lett., **65**(13), pp. 1629–1631.

[13] Kang, K., Koh, Y. K., Chiritescu, C., Zheng, X., and Cahill, D. G., 2008, "Two-Tint Pump-Probe Measurements Using a Femtosecond Laser Oscillator and sharp-Edged Optical Filters," Rev. Sci. Instrum., **79**(11), p. 114901.

[14] Qiu, T. Q., Juhasz, T., Suarez, C., Bron, W. E., and Tien, C. L., 1994, "Femtosecond Laser-Heating of Multilayer Metals. 2. Experiments," Int. J. Heat Mass Transfer, **37**(17), pp. 2799–2808.

[15] Thomsen, C., Strait, J., Vardeny, Z., Maris, H. J., Tauc, J., and Hauser, J. J., 1984, "Coherent Phonon Generation and Detection by Picosecond Light-Pulses," Phys. Rev. Lett., **53**(10), pp. 989–992.

[16] Rantala, J., Wei, L. H., Kuo, P. K., Jarrinen, J., Luukkala, M., and Thomas, R. L., 1993, "Determination of Thermal-Diffusivity of Low-Diffusivity Materials Using the Mirage Method With Multiparameter Fitting," J. Appl. Phys., **73**(6), pp. 2714–2723.

[17] Pottier, L., 1994, "Micrometer Scale Visualization of Thermal Waves by Photoreflectance Microscopy," Appl. Phys. Lett., **64**(13), pp. 1618–1619.

[18] Lepoutre, F., Balageas, D., Forge, P., Hirschi, S., Joulaud, J. L., Rochais, D., and Chen, F. C., 1995, "Micron-Scale Thermal Characterizations of Interfaces Parallel or Perpendicular to the Surface," J. Appl. Phys., **78**(4), pp. 2208–2223.

[19] Taketoshi, N., Ozawa, M., Ohta, H., and Baba, T., 1999, "Thermal Effusivity Distribution Measurements Using a Thermoreflectance Technique," *Photoacoustic and Photothermal Phenomena: Tenth International Conference*, F. Scudieri and M. Bertolotti, eds., AIP, New York.

[20] Hatori, K., Taketoshi, N., Baba, T., and Ohta, H., 2005, "Thermoreflectance Technique to Measure Thermal Effusivity Distribution With High Spatial Resolution," Rev. Sci. Instrum., **76**(11), pp. 114901.

[21] Schmidt, A. J., Cheaito, R., and Chiesa, M., 2009, "A Frequency-Domain Thermoreflectance Method for the Characterization of Thermal Properties," Rev. Sci. Instrum., **80**(9), pp. 094901.

[22] Capinski, W. S., and Maris, H. J., 1996, "Improved Apparatus for Picosecond Pump-and-Probe Optical Measurements," Rev. Sci. Instrum., **67**(8), pp. 2720–2726.

[23] Yarai, A., and Nakanishi, T., 2007, "Laptop Photothermal Reflectance Measurement Instrument Assembled With Optical Fiber Components," Rev. Sci. Instrum., **78**(5), p. 054903.

[24] Weaver, J. H., Lynch, D. W., Culp, C. H., and Rosei, R., 1976, "Thermoreflectance of V, Nb, and Paramagnetic Cr," Phys. Rev. B, **14**(2), pp. 459–463.

[25] Feldman, A., 1999, "Algorithm for Solutions of the Thermal Diffusion Equation in a Stratified Medium With a Modulated Heating Source," High Temp. - High Press., **31**(3), pp. 293–298.

[26] Incropera, F. P., and DeWitt, D. P., 1996, *Fundamentals of Heat and Mass Transfer*, Wiley, New York.

[27] Lee, S. M., and Cahill, D. G., 1997, "Heat Transport in Thin Dielectric Films," J. Appl. Phys., **81**(6), pp. 2590–2595.

[28] Yamane, T., Nagai, N., Katayama, S., and Todoki, M., 2002, "Measurement of Thermal Conductivity of Silicon Dioxide Thin Films Using a 3 Omega Method," J. Appl. Phys., **91**(12), pp. 9772–9776.

[29] Chien, H. C., Yao, D. J., Huang, M. J., and Chang, T. Y., 2008, "Thermal Conductivity Measurement and Interface Thermal Resistance Estimation Using SiO_2 Thin Film," Rev. Sci. Instrum., **79**(5), pp. 054902.

[30] Bao, Z. N., Feng, Y., Dodabalapur, A., Raju, V. R., and Lovinger, A. J., 1997, "High-Performance Plastic Transistors Fabricated by Printing Techniques," Chem. Mater., **9**(6), pp. 1299.

[31] Koh, Y. K., Singer, S. L., Kim, W., Zide, J. M. O., Lu, H., Cahill, D. G., Majumdar, A., and Gossard, A. C., 2009, "Comparison of the 3 Omega Method and Time-Domain Thermoreflectance for Measurements of the Cross-Plane Thermal Conductivity of Epitaxial Semiconductors," J. Appl. Phys., **105**(5), p. 054303.

[32] Cahill, D. G., and Pohl, R. O., 1987, "Thermal-Conductivity of Amorphous Solids Above the Plateau," Phys. Rev. B, **35**(8), pp. 4067–4073.

[33] Okuda, T., Nakanishi, K., Miyasaka, S., and Tokura, Y., 2001, "Large Thermoelectric Response of Metallic Perovskites: $Sr_{1-x}La_xTiO_3$ ($0 \Leftarrow x \Leftarrow 0.1$) ," Phys. Rev. B, **63**(11), pp. 113104.

[34] Shanks, H. R., Sidles, P. H., Maycock, P. D., and Danielson, G. C., 1963, "Thermal Conductivity of Silicon From 300 to 1400 Degrees K," Phys. Rev., **130**(5), pp. 1743–1748.

[35] Abramson, A. R., Kim, W. C., Huxtable, S. T., Yan, H. Q., Wu, Y. Y., Majumdar, A., Tien, C. L., and Yang, P. D., 2004, "Fabrication and Characterization of a Nanowire/Polymer-Based Nanocomposite for a Prototype Thermoelectric Device," J. Microelectromech. Syst., **13**(3), pp. 505–513.

[36] Stevens, R. J., Smith, A. N., and Norris, P. M., 2005, "Measurement of Thermal Boundary Conductance of a Series of Metal-Dielectric Interfaces by the Transient Thermoreflectance Technique," ASME J. Heat Transfer, **127**(3), pp. 315–322.